International Communications in Heat and Mass Transfer 37 (2010) 312–318

Contents lists available at ScienceDirect

International Communications in Heat and Mass Transfer

journal homepage: www.elsevier.com/locate/ichmt

CFD modeling of flow and heat transfer in a thermosyphon ☆

Asghar Alizadehdakhel [a], Masoud Rahimi [a,*], Ammar Abdulaziz Alsairafi [b]

[a] CFD Research Center, Chemical Engineering Department, Razi University, Kermanshah, Iran
[b] Faculty of Mechanical Engineering, College of Engineering and Petroleum, Kuwait University, Kuwait

ARTICLE INFO

Available online 22 October 2009

Keywords:
Thermosyphon
Heat pipe
CFD
Condensation
Evaporation

ABSTRACT

In the present study a gas/liquid two-phase flow and the simultaneous evaporation and condensation phenomena in a thermosyphon was modeled. The volume of fluid (VOF) technique was used to model the interaction between these phases. Experiments in a thermosyphon were carried out at different operating conditions. The CFD predicted temperature profile in the thermosyphon was compared with experimental measurements and a good agreement was observed. It was concluded that CFD is a useful tool to model and explain the complex flow and heat transfer in a thermosyphon.

1. Introduction

Heat pipes are two-phase heat transfer devices with extremely high effective thermal conductivity. The advantage of using the heat pipes is its need to small area and temperature difference. In addition, the simplicity of design, high rate of heat transfer, one way heat transfer (thermal diode), low cost, low weight, low cost of maintenance, etc. makes this equipment more demanding. In a heat pipe, heat is absorbed by the evaporator and transported to the condenser region where the vapor condenses by transferring heat to the cooling media. Heat pipes are known as efficient equipment for transferring heat and had significant development over half of century [1–3]. A heat pipe consists of an insulated pipe, a wick and working fluid. A group of heat pipes that fluid circulation happens inside them due to gravity called two-phase closed thermosyphon [3]. In this type of heat pipe, there isn't any wick for transferring the working fluid and fluid moves inside the pipe due to difference in its gravity. All heat pipes have three sections including: evaporator, adiabatic and condenser. In thermosyphons, the condenser always placed above the evaporator while in heat pipes with a wick in can be placed below the evaporator.

In a thermosyphon, the heat is inputted through the evaporator section where a liquid pool exists, turning the working fluid into vapor. The vapor rises and passes through the adiabatic section toward the condenser. In the condenser the vapor condenses and gives up its latent heat. Then, the condensate returns to the evaporator due to its gravity.

Regarding to their high efficiency, reliability and cost effectiveness, thermosyphons have been used in many different applications. These applications include preservation of permafrost, de-icing of roadways, turbine blade cooling, and applications in heat exchangers [4], humidity control [5], food industry [6], solar systems [7] and reactors [8], etc.

A numerous experimental and numerical investigations were carried out to understand the thermosyphons characteristics and the effect of various parameters on their performance. Liu et al. [9] studied visualization of the liquid flow in a two-phase closed thermosyphon using electrical capacitance tomography (ECT) with optimal step lengths for iterative image reconstruction algorithm. The enhancement of heat pipe thermal efficiency with nanofluids was investigated by Naphon et al. [10]. In their research the effects of amount of working fluid (fill ratio), heat pipe tilt angle and nanoparticles volume concentrations on the thermal efficiency of heat pipe were considered. Beside the experimental studies, substantial numerical works were carried out to predict and analyze the behavior of thermosyphones. Ghaddar [11] used a 2-D spectral element numerical model to investigate the hydrodynamic characteristics of a buoyancy-driven convection loop of an electrically conducting fluid in a transverse magnetic field. Numerical analysis of the effect of Rayleigh number and the aspect ratio on the performance of a C-shaped thermosyphones was presented by Mohammad and Sezai [12]. Basran and Kücüka [13] solved two-dimensional numerical models in the vertical heated and cooled sections of a thermosyphon loop using uniform wall temperature boundary condition. Results for laminar flow case were obtained by solving the momentum and the energy equations through the SIMPLEX Algorithm. Benne and Homan [14] employed a numerical method to analyze the behavior of a thermal storage device incorporating an integrated thermosyphon at constant heat flux with aim of accessing more uniform charge profile and decreasing the consequence of energy accumulation. Consequently, they developed their research by employing a constant temperature boundary condition [15].

The Computational Fluid Dynamics (CFD) is a powerful tool for fluid dynamics and thermal design in industrial applications, as well

☆ Communicated by W.J. Minkowycz.

* Corresponding author. Chemical Eng. Dept. Razi University, Taghe Bostan, Kermanshah, Iran.
E-mail address: masoudrahimi@yahoo.com (M. Rahimi).

0735-1933/$ – see front matter © 2009 Elsevier Ltd. All rights reserved.
doi:10.1016/j.icheatmasstransfer.2009.09.002

Nomenclature

C_p	heat capacity (J/kg K)
E	total energy per unit mass (J/kg)
ΔH	vaporization enthalpy (J/kg)
p	pressure (Pa)
q_j	xj-direction conductive heat flux (J/m^2 s)
Q_{in}	input energy to the evaporator (W)
Q_{out}	heat absorbed in the condenser (W)
S_E	energy source term (J/m^3 s)
S_F	momentum source term (kg/m^2 s^2)
S_M	mass source term (kg/m^3 s)
T	temperature (K)
T_c	cooling water inlet temperature (K)
T_h	cooling water outlet temperature (K)
T_{sat}	saturation temperature (K)
t	time (s)
u_i	xi-direction velocity component (m/s)
u_j	xj-direction velocity component (m/s)
$\dot{V}$	cooling water flow rate of (m^3/s)
x_{water}	volume fraction of water in gas phase

Greek letters

α_k	volume fraction of phase k
δ_{ij}	Kronecker function
μ	dynamic viscosity (Pa s)
μ_k	dynamic viscosity of phase k (Pa s)
η	performance of thermosyphon
ρ	density (kg/m^3)
ρ_k	density of phase k (kg/m^3)

as in academic research activities [16,17]. Multi-phase flows have received growing research attention among CFD practitioners due, in large measure, to the evolving maturity of single-phase algorithms that have been adapted to the increased complexity of multi-component systems. Gan et al. [18] presented the results of experimental measurement and numerical simulation of the performance of a heat pump system designed to make use of rainwater and ground as heat sources/sinks. A finite difference method and a CFD modeling was used to predict fluid flow, conduction and convection heat transfer.

Modeling of gas–liquid interface is quite important in the prediction of interphase heat and mass transfer. Some researchers found that the Volume Of Fluid (VOF) model is more suitable for simulating interface between two or more fluids. Ghorai and Nigam [19] used commercial CFD code, FLUENT 6.0, to model gas/liquid two-phase flow in a pipe. The VOF technique was employed and the gas velocity, the liquid volume fraction and interfacial roughness were treated as studied variables. They validated their modeling by comparing the predicted interfacial roughness with data in the literature.

Lu et al. [20] employed the VOF technique to model gas–liquid flow in a large scale horizontal pipe with an inner diameter $D=125$ mm. The two-phase flow regimes and the regime transition from stratified to slug flow were investigated. They compared the obtained results with experimental observations and reported a good agreement.

De Schepper et al. [21] used VOF model to predict the two-phase co-current horizontal gas–liquid and vapor–liquid flow regimes in a tube. They compared the CFD predicted results with Baker chart and concluded that all horizontal flow regimes appearing in the Baker chart can be simulated using existing CFD codes. In another research presented by De Schepper et al. [22], a model was developed to simulate the flow boiling process of a hydrocarbon feedstock in the convection section of a steam cracker. They used the VOF model to simulate different horizontal two-phase flow regimes evolve with flow boiling. The heating and boiling phenomena were modeled by implementing the appropriate source terms in the conservation equations. These source terms, describing the mass and heat transfer during the evaporation process, was derived from the Hertz–Knudsen equation.

Regarding to the above mentioned investigations for modeling of the two-phase or phase change using CFD, in the present work it has been tried to model a combination of the two-phase flow with evaporation and condensation in a thermosyphon. For this purpose, a set of experiments in a closed two-phase thermosyphon were carried out to investigate its performance in different operating conditions. The CFD modeling was carried out to show the ability of this technique for this purpose as well as to explain the experimental observations.

2. Theory

The VOF method [23] relies on the fact that two or more phases are not interpenetrating and for each additional phase the volume fraction of the phase must be added in the computation. In the VOF model, the sum of the volume fractions of all phases in each control volume is equal to one. In the CFD modeling, the Navier–Stokes equations are solved simultaneously. These equations are as follows:

Continuity:

$$\frac{\partial}{\partial t}(\rho) + \sum_{j=1}^{3}\frac{\partial}{\partial x_j}(\rho u_j) = S_M \tag{1}$$

Momentum:

$$\frac{\partial}{\partial t}(\rho u_i) + \sum_{j=1}^{3}\frac{\partial}{\partial x_j}(\rho u_i u_j) = -\frac{\partial p}{\partial x_i} + \sum_{j=1}^{3}\frac{\partial}{\partial x_j}\left[\mu\left(\frac{\partial u_i}{\partial x_j} + \frac{\partial u_j}{\partial x_i} - \frac{2}{3}\delta_{ij}\sum_{i=1}^{3}\frac{\partial u_i}{\partial x_i}\right)\right] + S_{F,i} \tag{2}$$

Energy:

$$\frac{\partial}{\partial t}(\rho E) + \sum_{j=1}^{3}\frac{\partial}{\partial x_j}(\rho E u_j) = \sum_{i=1}^{3}\sum_{j=1}^{3}\left(\frac{\partial}{\partial x_j}(\tau_{ij})u_i\right) - \sum_{j=1}^{3}\frac{\partial}{\partial x_j}q_j + S_E \tag{3}$$

In these equations, the density (ρ) and viscosity (μ) of the fluid depend on the volume fractions of each phase (α_k) and they are calculated by the following equations:

$$\rho = \sum_{k=1}^{2}\alpha_k\rho_k \tag{4}$$

$$\mu = \sum_{k=1}^{2}\alpha_k\mu_k \tag{5}$$

The VOF model treats energy (E) and temperature (T) as mass-averaged variables:

$$E = \frac{\sum_{k=1}^{2}\alpha_k\rho_k E_k}{\sum_{k=1}^{2}\alpha_k\rho_k} \tag{6}$$

Where E_k for each phase is based on the specific heat of that phase and the shared temperature. The interface between two phases is tracked by the volume fraction. Conservation of α can be represented by the interface mass balance using the following equation:

$$\frac{\partial\alpha}{\partial t} + u.\nabla\alpha = 0 \tag{7}$$

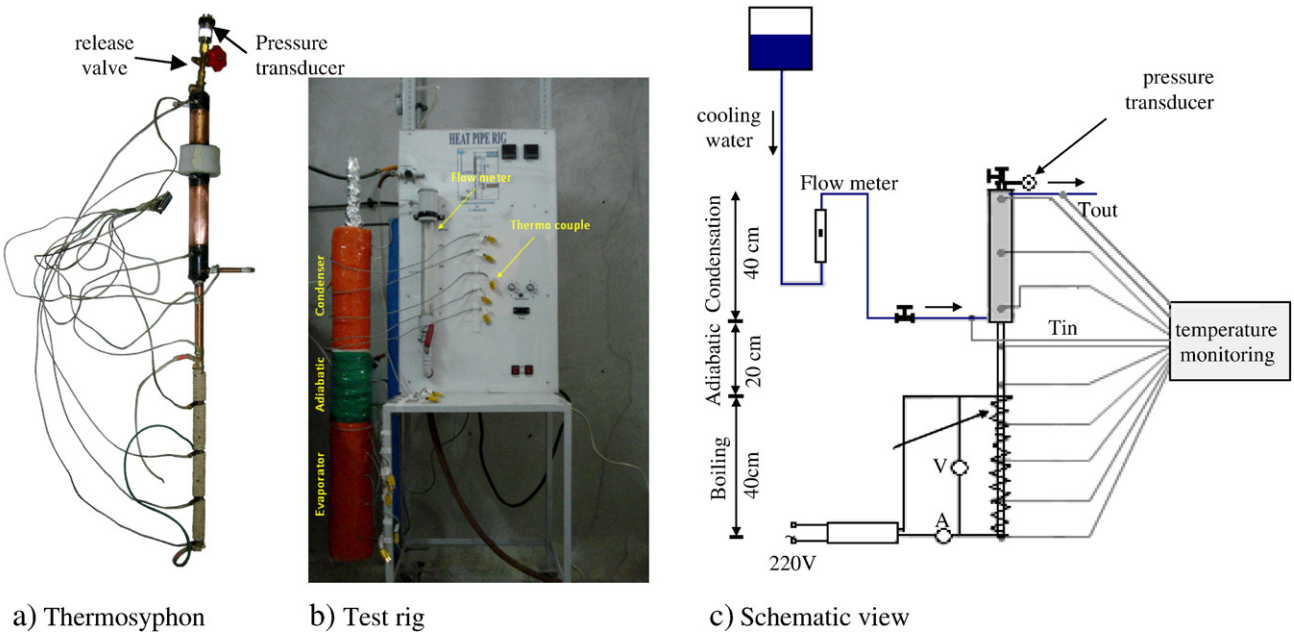

Fig. 1. Experimental setup.

The cell phase is vapor where $\alpha=1$, while $\alpha=0$ means that the whole volume has been occupied by the liquid. It can be concluded that the vapor/liquid interface exists in the regions that α lies between zero and one. When the temperature of liquid phase exceeds the saturation temperature, T_{sat}, mass with rate of S_M transfers from liquid phase to the vapor phase and an amount of E energy is absorbed.

3. Experiments

3.1. Experimental aspects

The experiments were carried out in a vertical thermosyphon and its performance in different inputted energy to the evaporation section and fill ratios was studied. A closed copper tube with a length of 100 cm and inner and outer diameters of 1.75 and 19 cm was used as the thermosyphon. The condenser section was constructed from a cylindrical shell with a length of 40 cm that surrounded the upper region of the thermosyphon and cooling water was introduced to it in upward direction. The flow rates of the cold water were controlled by a valve and measured by a flow meter with an accuracy of ±0.2% of full scale. A length of 40 cm from bottom of the thermosyphon was used as the evaporation section and energy was transferred to it by an electrical heater with a predefined power input. The heat input to the evaporator was set using an electrical energy regulator (Variac). Ten thermocouples were placed on the tube to measure the temperature of evaporator, adiabatic and condenser sections. The thermocouples used in the experiment had a measurement error of ±0.5 °C. Two other thermocouples were used to measure the inlet and outlet temperatures of the cooling water. The uncertainty of the measurement for flowmeters and thermometers was ±0.01 and ±0.1, respectively.

The experimental rig and a schematic view of the experimental setup are shown in Fig. 1. Three different inlet heat flow rates of 700, 500 and 350 W and three different fill ratios (the ratio of initial liquid volume per total volume of evaporation section) of 0.3, 0.5 and 0.8 were examined.

3.2. Experimental results

Measured temperature variations along the thermosyphon at different inlet heat flow rates for fill ratio (FR = 0.5) are shown in Fig. 2. The figure indicates that temperature profile along the tube has a similar trend for different inlet heat fluxes. The results show higher established temperature at the evaporator decreased as passing trough adiabatic and condenser section. In addition, the effect of increasing the inlet heat flow on the wall temperature is more significant in the evaporation section rather than the adiabatic and condensation sections.

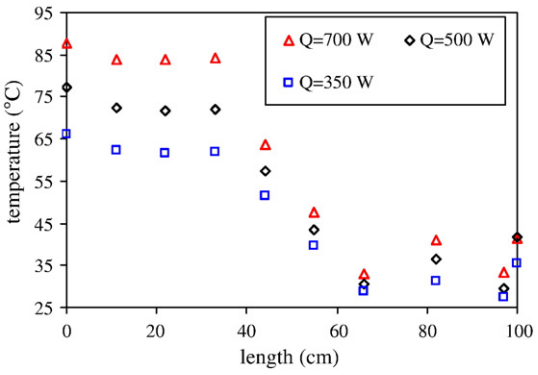

Fig. 2. Temperature variations along the thermosyphon at different inlet heat flow rates (FR = 0.5).

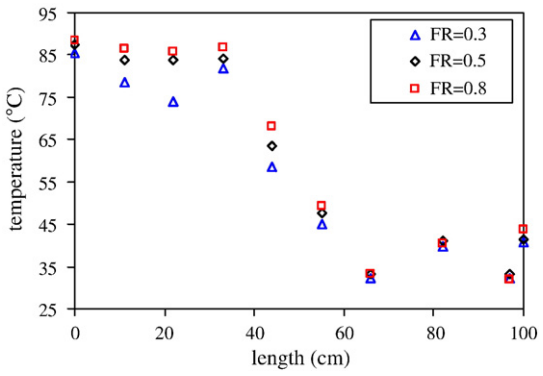

Fig. 3. Tube wall temperatures at various fill ratios.

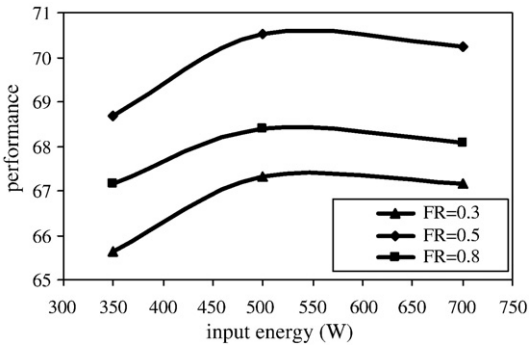

Fig. 4. The thermosyphon performances at various energy inputs and fill ratios.

In addition, rising temperature trend happened at the upper region of condenser, more obviously at higher heat input to the evaporator.

The effect of fill ratio on the established temperature profile on the thermosyphon is shown in Fig. 3. It can be seen that the wall temperatures in the condenser region are almost the same for the three cases. However, in the evaporation section, the temperature increases by increasing the fill ratio.

The heat performance is one of the most important characteristics in a thermosyphon and has been defined as the ratio of heat absorbed by the condenser section to the energy introduced to the evaporation section as follow:

$$\eta = \frac{Q_{out}}{Q_{in}} * 100 \tag{8}$$

Where, Q_{out}, the amount of heat absorbed by the cooling water in the condenser section can be calculated using the following relation:

$$Q_{out} = \rho \dot{V} c_p (T_h - T_c) \tag{9}$$

In which ρ is the density, $\dot{V}$ is the volumetric flow rate and C_P is the heat capacity of cooling water. In addition, T_c and T_h are the inlet and outlet temperatures of cooling water, respectively.

The performance of thermosyphon at different heat inputs and fill ratios are calculated and plotted in Fig. 4. From this figure, the maximum performance can be observed at input energy of 500 W for all examined fill ratios. In addition, the results show that the fill ratio has a significant effect on performance of thermosyphon and in this study the best performance was obtained at fill ratio of 0.5.

4. CFD modeling

The 2-D CFD analysis presented in this study was completed using FLUENT™ version 6.2.The CFD package was used to model the gas–liquid as well as phase change during evaporation and condensation inside the thermosyphon.

4.1. Mesh geometry

A 2-D geometry with specific grids near the walls was provided for modeling of flow, heat and mass transfer within the thermosyphon. Fig. 5 shows the used geometry and created grids on it. The evaporator, condenser and adiabatic sections are indicated in the figure. The boundary layer technique of Gambit software was used to mesh near-wall regions of the thermosyphon. Five rows of mesh with initial size of 0.1 mm and growth factor of 1.2 was used. A total number of 47,124 grids were created in the fluid region of the domain and 14,361 grids were used for the solid (walls) region.

4.2. Initial and boundary conditions

The fill ratios were applied by patching liquid volume fraction of unity for heights of the evaporator proportional to the fill ratios for each case. In the gas phase, according to the experiments, the initial mole fraction of water vapor was set to the ratio of vapor pressure of water at 15 °C (1.72 kpa) to the total initial pressure of 20 kpa for all cases based on measured values from experiments. According to the experiments, three different values of 14,659, 20,941.5 and 29,318 W/m^2 (related to 350, 500 and 700 W) were applied as energy inlet to the evaporator and energy outlet from the condenser. The gravity acceleration of 9.8 m/s^2 was used as body force source term.

4.3. Solution techniques

The VOF model was employed for two-phase flow modeling. Liquid water was defined as the secondary (liquid) phase and the following equation driven from the steam table was used for its density:

$$\rho_{liq} = -0.0022 \times T^2 + 0.9237 \times T + 919.8 \tag{10}$$

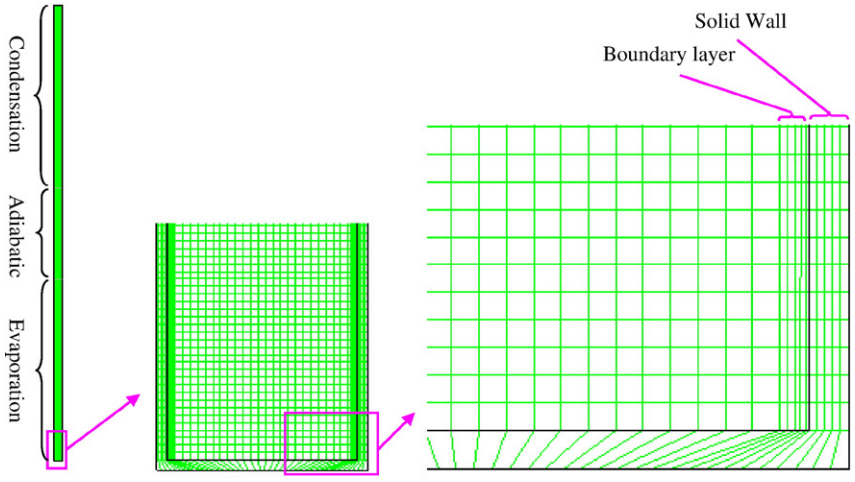

Fig. 5. The employed mesh geometry in the modeling.

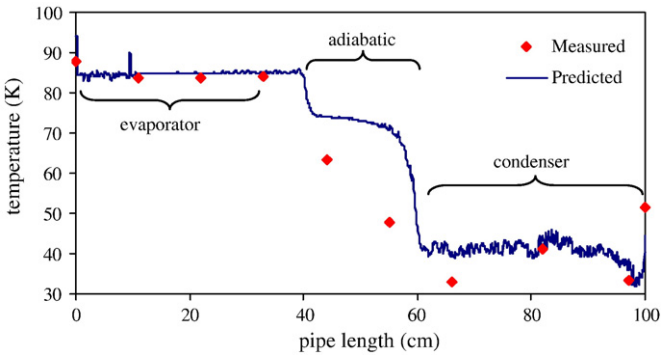

Fig. 6. The comparison between CFD predicted and measured temperatures.

For the evaporation process, equations proposed by De Schepper et al. [22] were used to calculate the source terms:

Liquid phase:

$$S_M = -0.1\alpha_{liq}\rho_{liq}\left|\frac{T_{liq}-T_{sat}}{T_{sat}}\right| \quad (11)$$

Vapor phase:

$$S_M = 0.1\alpha_{liq}\rho_{liq}\left|\frac{T_{liq}-T_{sat}}{T_{sat}}\right| \quad (12)$$

Energy:

$$S_E = -0.1\alpha_{liq}\rho_{liq}\left|\frac{T_{liq}-T_{sat}}{T_{sat}}\right| \Delta H \quad (13)$$

In order to completely model the condensation process, the effect of non-condensable gases must be considered. A mixture of air and water vapor was used as the primary (gas) phase. The source terms proposed by De Schepper et al. [22] were modified as follows in order to model the condensation phenomena considering the effect of non-condensable gases:

Liquid phase:

$$S_M = 0.1x_{water}\alpha_{vap}\rho_{vap}\left|\frac{T_{vap}-T_{sat}}{T_{sat}}\right| \quad (14)$$

Vapor phase:

$$S_M = -0.1x_{water}\alpha_{vap}\rho_{vap}\left|\frac{T_{vap}-T_{sat}}{T_{sat}}\right| \quad (15)$$

Energy:

$$S_E = 0.1x_{water}\alpha_{vap}\rho_{vap}\left|\frac{T_{vap}-T_{sat}}{T_{sat}}\right| \Delta H \quad (16)$$

Where, x_{water} is the volume (mole) fraction of water vapor in the gas phase. User define subroutines (UDF) were developed to employ these equations for modeling of the boiling and condensation phenomena. Phase change was considered to occur at the boiling temperature of 350 K. The UDFs linked to main hydrodynamic model equations of the commercial CFD software, Fluent 6.2 to model the heat and mass transfer in the thermosyphon. The species model of Fluent was used to treat the mixture of air and water vapor. The surface tension was implemented using the method of Brackbill et al. [24].

Because of the dynamic behavior of the two-phase flow, unsteady state calculations with a time step of 0.001 s were carried out for all

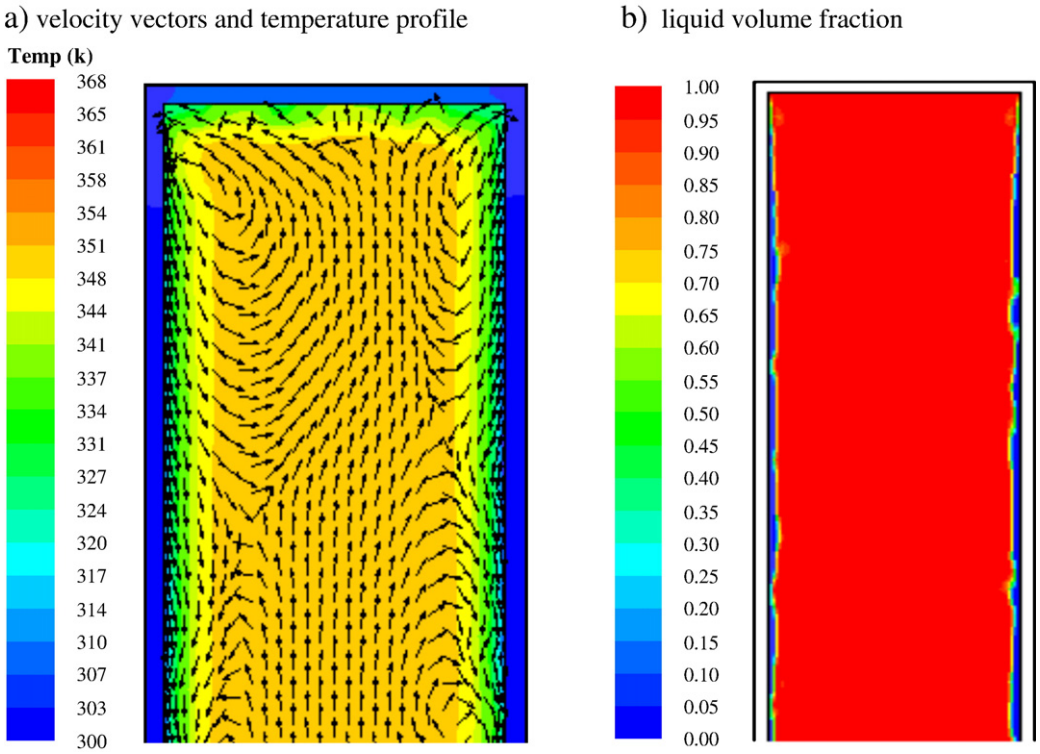

Fig. 7. The CFD predicted fluid flow, temperature and condensation at top of the condenser.

cases. The calculations were performed by combination of the SIMPLE algorithm for pressure–velocity coupling, first order upwind calculation scheme for the discretization of momentum and energy equations and Geo-Reconstruct for the volume fraction. The convergence criterion was based on the residual value of the calculated variables, namely mass, velocity components and volume fraction. In the present calculations, the numerical computation was considered converged when the scaled residuals of the different variables are lowered by four orders of magnitude. The calculations were continued for three minutes and the semi-steady state results were analyzed.

5. Results and discussion

A comparison between CFD predicted and measured temperature profile along the thermosyphon wall is given in Fig. 6. A reasonable agreement can be observed between measured and predicted data except in the adiabatic section. This difference can be explained by the fact that in the experiments, there is some energy loses in the adiabatic section, while it is ignored in the modeling. Therefore, the values of temperature in adiabatic section are over predicted. In the other words, applying the adiabatic condition in the modeling causes the temperature to be constant in this section in the predicted results.

As previously illustrated in Figs. 2 and 3, the measured wall's temperature rises at the top region of the condensation section. The velocity vectors and contour plots of temperature and volume fraction are presented in Fig. 7 to explain this experimental observation. Fig. 7 shows that saturated steam flows upward from the center of the tube, meets the top wall and cause an increase in the wall temperature. In addition, from liquid volume fraction contour plot presented in Fig. 7(b) it can be found that the thickness of liquid film near the wall is lower at the upper side and increases as the liquid flows downward. Lower liquid thickness at the upper side can causes a decrease in liquid film thermal resistance. Therefore, the convection heat transfer from this side to the lateral wall is higher than those of lower regions of the condenser. This can be the reason for higher observed wall's temperatures at the upper side of the condenser.

In order to explain the changes in efficiency at various heat input using the CFD predicted results, the values of liquid volume fraction at various distances from the wall for the three examined heat inputs to the evaporator are plotted in Fig. 8. By more contrast on the condensation section, from 60 to 100 cm illustrated in this figure, it can be found that when the applied energy rate of 350 W was established, the liquid volume fraction along the thermosyphon inner wall is quite negligible. Fig. 8(a) reveals that it is possible to find a very thin layer, almost 0.2 mm, close to the wall. It means there are significant dry areas in the condensation section and heat transfer occurred with free convection mechanism instead of a higher heat transfer rate due to condensation mechanism. Fig. 8(b) also shows that a thinner layer of liquid formed near the wall when the applied inlet flow is 500 W. This prediction shows that in this condition, a higher rate of condensation occurred along whole condenser surface. By applying more heat to the evaporator a thick liquid layer established in the condensation section, as illustrated in Fig. 8(c). Increasing the thickness of liquid layer can cause higher thermal resistance and consequent lower heat transfer coefficient. Decreasing the capability of heat absorption in the condensation section can decrease the thermal efficiency of thermosyphon as it was found in the experiments for the 700 W heat input to the evaporator, shown in Fig. 4.

On the other hand, the effect of fill ratio on experimental evaluated thermosyphon efficiency was previously shown in Fig. 4. That measured results showed that the thermosyphon performance increased as fill ratio increased from 0.3 to 0.5. However, a decrease in its performance observed by increasing the fill ratio from 0.5 to 0.8. In order to explain this observation, in Fig. 9, as an example, the contour plot of vapor phase formed for the 0.8 fill ratio is illustrated.

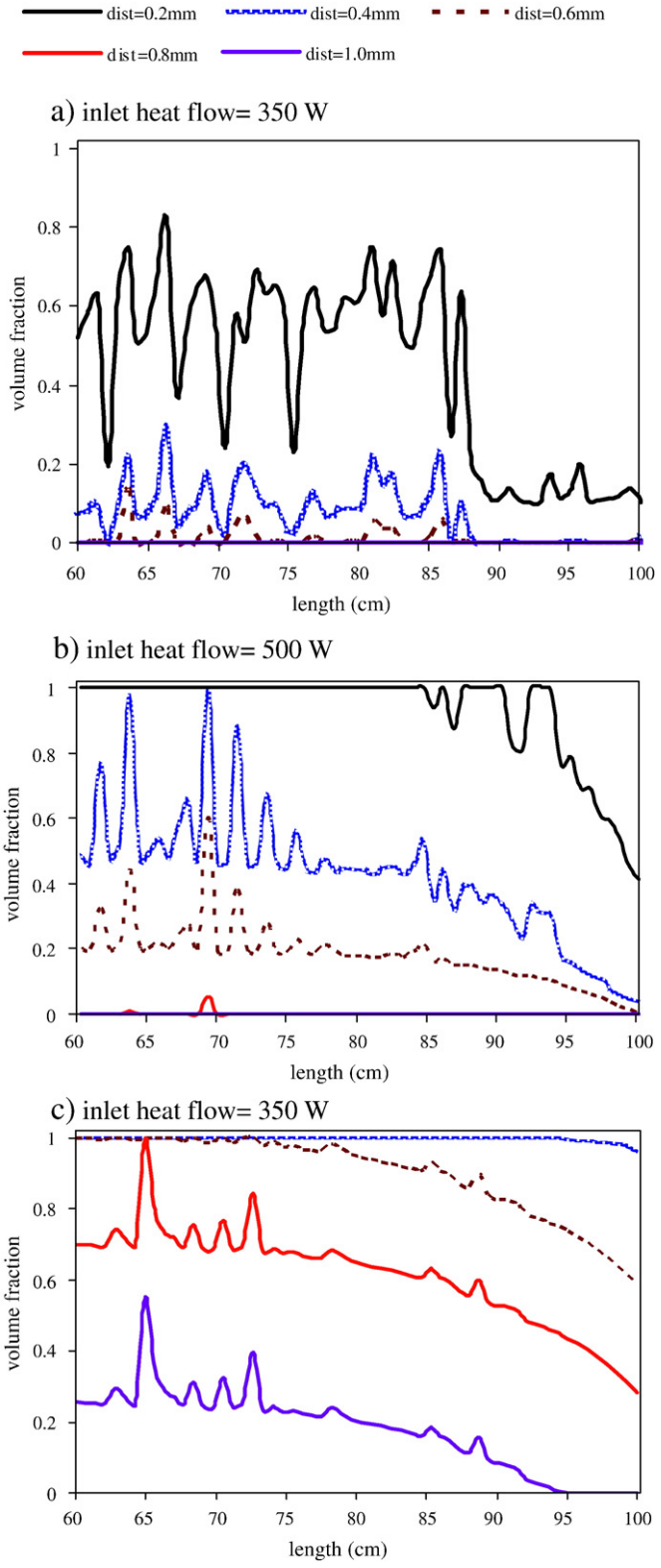

Fig. 8. Liquid volume fraction close to the thermosyphon wall.

The figure shows that in the bottom section of the evaporator, the generated thick layers of vapor are stuck to the wall. Because of a low thermal conductivity of vapor, these thick vapor layers can cause a significant thermal resistance and consequently decrease the overall heat transfer coefficient. However, in upper region of evaporator the vapor layers become smaller. In addition, close to the evaporator

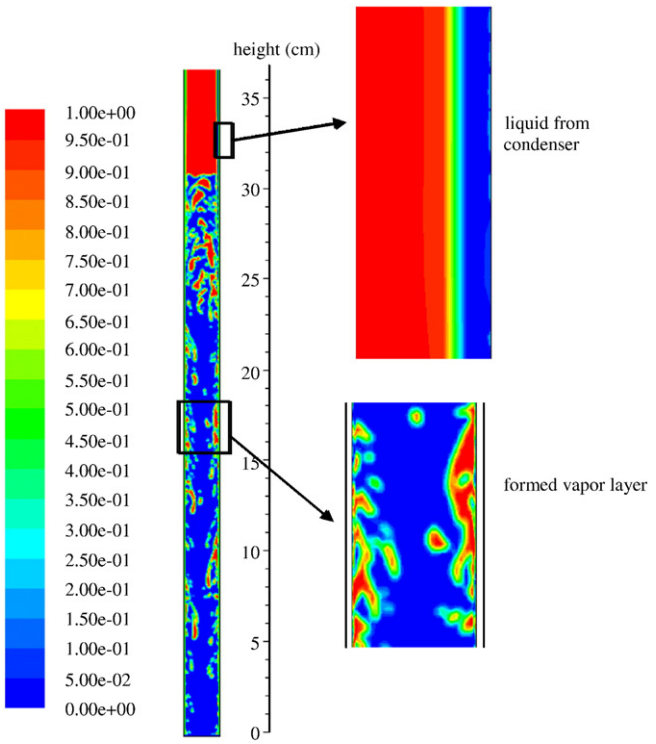

Fig. 9. Contour plots of vapor volume fraction in the evaporation section (FR = 0.8).

liquid surface the bubbles moves toward the middle regions of the liquid pool for escaping from liquid surface.

From above discussion it can be concluded that increasing the fill ratio has two opposite effects on the rate of evaporation. First, at higher fill ratio it is possible to have more heat transfer from the evaporator wall to the working fluid, as more evaporator's wall surface is in contact with the working fluid. This can increase the evaporation rate and consequent thermosyphon performance. However, as shown in Fig. 9, higher height of working fluid has a negative effect of large bubbles or film formation in the lower parts of the evaporator. This has direct effect on heat transfer rate to the evaporator and can decrease the thermosyphon performance. Therefore, the fill ratio for a thermosyphon can has an optimum value as it is 0.5 for the studied thermosyphon in the range of the measured heat load and fill ratios.

6. Conclusion

In the present study, experiments in a thermosyphon were carried out in order to investigate the effect of input heat flow and fill ratio on the performance of the thermosyphon. The experimental results showed that increasing of the inlet heat flow from 350 to 500 increases the thermosyphon's performance. However, applying higher energy to the evaporator decreases the performance. In addition, it was found that there is an optimum value of the fill ratio for each value of input energy to the evaporation section. A UDF subroutine was developed to model the phase change using Fluent 6.2 commercial CFD code. A good agreement was observed between CFD predicted and measured temperature profiles. The CFD results were employed to understand the reasons for the observed changes in the temperature profiles and performance of the thermosyphon. The results of this investigation showed that the complex heat and mass transfer encountered phase change can be successfully modeled using CFD technique.

Acknowledgment

The authors wish to express their thanks to the Iranian National Gas company-Kermanshah province for the financial support of this work.

References

[1] R.S. Gauglar, Heat transfer device, US patent 2350348, 1942.
[2] G.M. Grover, Evaporation–condensation heat transfer device, US patent 3229759, 1963.
[3] G.P. Peterson, An Introduction to Heat Pipes, Modeling, Testing and Applications, John Wiley & Sons Inc., New York, USA, 1994.
[4] A. Faghri, Heat Pipe Science and Technology, Taylor & Francis, Washington DC, USA, 1995, p. 341.
[5] X.P. Wu, P. Johnson, A. Akbarzadeh, Application of heat pipe heat exchangers to humidity control in air-conditioning systems, Applied Thermal Engineering 17 (6) (1997) 561–568.
[6] A.K. Silva, M.B.H. Mantelli, Thermal applicability of two-phase thermosyphons in cooking chambers—experimental and theoretical analysis, Applied Thermal Engineering 24 (5–6) (2004) 717–733.
[7] S.L. Abreu, S. Colle, An experimental study of two-phase closed thermosyphons for compact solar domestic hot-water systems, Solar Energy 76 (1–3) (2004) 141–145.
[8] A.K. Nayak, D. Lathouwers, T.H.J.J. van der Hagen, F. Schrauwen, P. Molenaar, A. Rogers, A numerical study of boiling flow instability of a reactor thermosyphon system, Applied Thermal Engineering 26 (5–6) (2006) 644–653.
[9] S. Liu, J. Li, Q. Chen, Visualization of flow pattern in thermosyphon by ECT, Flow Measurement and Instrumentation 18 (5–6) (2007) 216–222.
[10] P. Naphon, P. Assadamongkol, T. Borirak, Experimental investigation of titanium nanofluids on the heat pipe thermal efficiency, International Communications in Heat and Mass Transfer 35 (10) (2008) 1316–1319.
[11] N.K. Ghaddar, Numerical simulation of a vertical themosyphonic loop placed in a transverse magnetic field, Numerical Heat Transfer. Part B, Fundamentals 32 (2) (1997) 231–246.
[12] A.A. Mohamad, I. Sezai, Natural convection in C-shaped thermosyphon, Numerical Heat Transfer. Part A, Applications 32 (3) (1997) 311–323.
[13] T. Basran, S. Kücüka, Flow through a rectangular thermosyphon at specified wall temperatures, International Communications in Heat and Mass Transfer 30 (7) (2003) 1027–1039.
[14] K.S. Benne, K.O. Homan, Dynamics of closed-loop thermosyphon incorporating thermal storage, Numerical Heat Transfer. Part A, Applications 54 (3) (2008) 235–254.
[15] K.S. Benne, K.O. Homan, Transient behavior of thermosyphon-coupled sensible storage with constant temperature heat addition, Numerical Heat Transfer. Part A, Applications 55 (2) (2009) 101–123.
[16] S.B. Riffat, G. Gan, Determination of effectiveness of heat-pipe heat recovery for naturally-ventilated buildings, Applied Thermal Engineering 18 (3–4) (1998) 121–130l.
[17] G. Gan, S.B. Riffat, A numerical study of solar chimney for natural ventilation of buildings with heat recovery, Applied Thermal Engineering 18 (12) (1998) 1171–1187.
[18] G. Gan, S.B. Riffat, C.S.A. Chong, A novel rainwater-ground source heat pump—measurement and simulation, Applied Thermal Engineering 27 (2–3) (2007) 430–441.
[19] S. Ghorai, K.D.P. Nigam, CFD modeling of flow profiles and interfacial phenomena in two-phase flow in pipes, Chemical Engineering and Processing Journal 45 (1) (2006) 55–65.
[20] G. Lu, J. Wang, Z. Jia, Experimental and numerical investigations on horizontal oil-gas flow, Journal of Hydrodynamics 19 (6) (2007) 683–689.
[21] S.C.K. De Schepper, G.J. Heynderickx, G.B. Marin, CFD modeling of all gas–liquid and vapor–liquid flow regimes predicted by the Baker chart, Chemical Engineering Journal 138 (1–3) (2008) 349–357.
[22] S.C.K. De Schepper, G.J. Heynderickx, G.B. Marin, Modeling the evaporation of a hydrocarbon feedstock in the convection section of a steam cracker, Computers & Chemical Engineering 33 (1) (2009) 122–132.
[23] C.W. Hirt, B.D. Nichols, Volume of Fluid (VOF) method for the dynamics of free boundaries, Journal of Computational Physics 39 (1) (1981) 201–225.
[24] J.U. Brackbill, D.B. Kothe, C. Zemach, A continuum method for modelling surface tension, Journal of Computational Physics 100 (2) (1992) 335–354.